Applying Stochastic Models to Analyze Vibration Features of Roller Bearings

Saima Bhatti , ASIF Ali Shaikh , Asif Mansoor * , Murtaza Hussain

Posted Date: 18 August 2023

doi: 10.20944/preprints202308.1287.v1

Keywords: Machinery, Prognosis framework, Vibration data, Roller bearings, Stochastic models

Article

Applying Stochastic Models to Analyze Vibration Features of Roller Bearings

Saima Bhatti [1], Asif Ali Shaikh [1], Asif Mansoor [2,*]and Murtaza Hussain [2]

[1] Department of Basic Sciences and Related Studies, Mehran University of Engineering and Technology, Jamshoro, 76060, Pakistan

[2] National University of Sciences & Technology, Islamabad, 44320, Pakistan

* Correspondence: drasifmansure@pnec.nust.edu.pk; Tel.: +923012990882

Abstract: Machinery parts gradually wear out over time due to regular usage. To improve machinery health and prevent critical issues, a reliable prognosis framework can be implemented by monitoring the behaviour of machinery parts and issuing warnings before they reach a critical state. To achieve this, vibration data from roller bearings experiencing various fault conditions have been collected. Different techniques from the literature were combined to analyze the distinct configurations in the vibration data sets and identify the main defects in roller bearings. The significant features extracted from this analysis were then used to create optimized stochastic model equations, separately regressing inner and outer race fault features to healthy bearing features under random conditions. These models can help engineers design more dependable systems, optimize their performance, and minimize the risk of failures and downtime.

Keywords: machinery; prognosis framework; vibration data; roller bearings; stochastic models

1. Introduction

The physical condition of rolling element bearings plays a crucial role in ensuring the safe and efficient operation of rotating machinery. Rolling bearing failures contribute to more than 40% of all failures in such equipment [1]. Therefore, monitoring their condition and implementing intelligent and reliable diagnosis methods is vital for system design and maintenance. As a result, extensive research has been devoted to these critical aspects over the past few decades [2–9].

Fault diagnosis for rotating equipment can be considered as identifying patterns in the data. The process usually involves two main steps: extracting relevant features from the data and classifying the faults. Vibration-based signal processing is a widely used approach for the first step, where the data is analyzed in the time domain, frequency domain, or time-frequency domain.

Bearing signals are intrinsically dynamic, making them almost always non-stationary. This non-stationary behaviour can be caused by abrupt changes in the signal resulting from the clearance between the bearing outer race and the housing or sliding of a rolling element. Additionally, impacts of the damaged and non-damaged parts of a bearing or flaking of one of the bearing raceways can also cause non-stationarities. Traditional non-parametric techniques like the FFT have limitations in dealing with non-stationary signals, as they require long time intervals to form a good resolution spectrum and are not suitable for non-stationary signals. To address these limitations, many studies have proposed methods such as analyzing the signal instantaneously in its time and frequency domain using short-term Fourier transform and wavelet transform. Although these methods provide an overall view of non-stationary signals in time-frequency domains, they may not always obtain good frequency resolution. Some studies involve transformations aimed at decomposing the signal into simpler components, such as empirical mode decomposition, which can be more complicated than the proposed differencing procedure [10–16].

Stochastic approaches are also utilized in the analysis of bearing inner race and outer race faults. These approaches utilize probabilistic techniques to represent the uncertainties associated with the bearing's operation and the occurrence of faults.

One of the most common stochastic models is the Markov chain model. This model assumes that the bearing's health status can be described by a finite number of discrete states, such as healthy,

Preprints (www.preprints.org) | NOT PEER-REVIEWED | Posted: 18 August 2023 doi:10.20944/preprints202308.1287.v1

incipient fault, and severe fault. The transition probabilities between these states are determined based on the bearing's operating conditions and the characteristics of the fault. Another stochastic model used in bearing fault analysis is the hidden Markov model (HMM). This model considers that the bearing's health status cannot be directly observed but can only be inferred from observable data, such as vibration signals or acoustic emissions. The HMM assumes that the bearing's health status follows a hidden state process that can be modelled by a Markov chain, and the observable data is generated based on the current hidden state [17–28].

In this study, the stochastic resonance approach is utilized to extract the feature of the faulty bearing under different experimental conditions, which utilizes random noise in the detection of faults. The extracted feature detects the presence of various defects in bearings, including spalls, cracks, wear, and other types of faults. These monitored features are utilized to develop the stochastic equation to describe the uncertainties that occur in the working condition of the system. These developed equations will help to detect and repair faulty bearings before they cause a catastrophic failure.

2. Experimental Set-up

The bearing datasets used in this research paper were obtained through experimentation conducted on a Bearing failure test rig, as depicted in Figure 2. To collect bearing failure data with an induced nonlinearity (i.e., defect), an accelerated testing concept was employed. The primary focus of the experimentation was to observe the trend following the induction of the defect until the failure threshold was reached, allowing for the estimation of the remaining useful life, also known as the P-F interval.

The test rig utilized a simple arrangement, driven by a two HP variable speed induction motor. A specifically designed shaft was then supported by two bearings. The test bearing, SKF6209, was subjected to both radial and axial loading under defect conditions. A screw-type loading mechanism was implemented to apply static load in the radial direction, while axial loading was induced randomly using a modal exciter. Instantaneous peak values were acquired using a portable vibration analyzer, and a series of real-time data was also collected using an NI DAQ system.

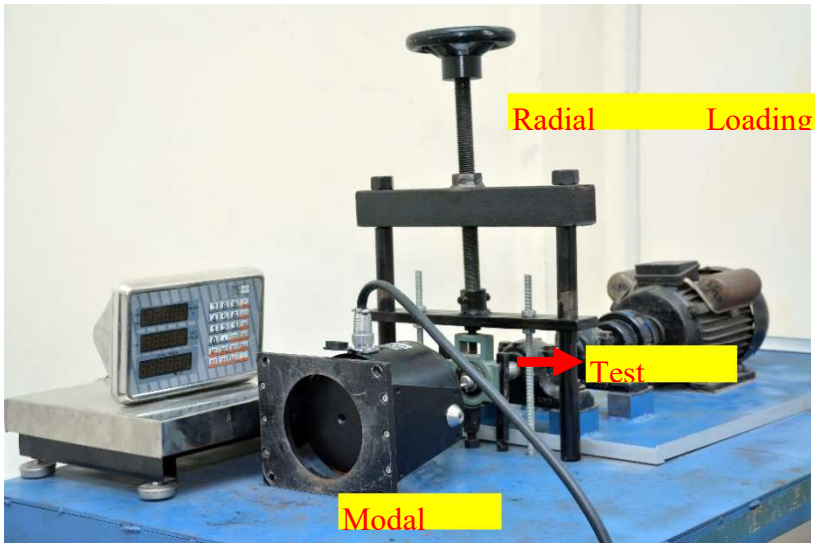

Figure 1. Experimental Setup.

The experimental conditions at various loadings with different bearing defects are listed in Table 1.

Preprints (www.preprints.org) | NOT PEER-REVIEWED | Posted: 18 August 2023 doi:10.20944/preprints202308.1287.v1

Table 1. Experimental condition.

S.No	Redial Loding(mm)	Defect Width (mm)	Defect Depth (mm)
1	30	38	12
2	45	38	12
3	60	38	12

To enhance feature extraction and facilitate the development of reliable prognostic models, the peak values of defect frequencies were pickedr. This approach aimed to eliminate the influence of noise that could potentially mask the relevant frequencies within the overall spectral energy. By focusing on the peak values, a clearer understanding of the specific defect propagation could be achieved. For this study, we specifically concentrated our efforts on localizing the analysis to the peak values associated with the Outer Race defect.

3. Spectral Analysis

The SKF 6209 test bearing underwent various loadings as outlined in Table 2. During the initial 20 hours of running, the vibration levels remained stable, and no significant defect frequencies were observed. Subsequently, after approximately 10 more hours of bearing operation under a radial load of 45 N, along with variable axial loading, defect frequencies related to inner race damage were detected, accompanied by a slight increase in vibration levels.

As the bearing further progressed in its failure state, outer race defects became evident. At this stage, the vibration signal displayed a distinct periodicity due to the impacts generated by metal-to-metal contact. However, in the later stages of fault, the periodic impulses were obscured by the noise energy resulting from the propagated defect across the bearing's outer race. Spectral results for the SKF 6209 bearing under a 45 N load at different stages are depicted in Figures. 2a to 2c for reference.

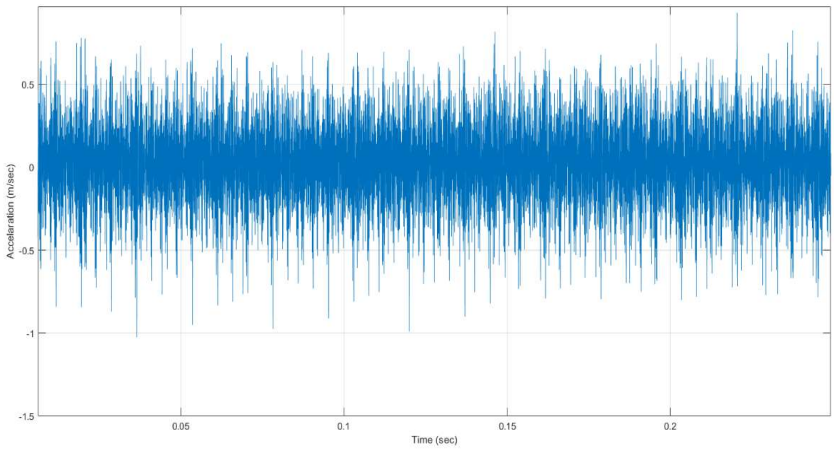

(2a) Healthy Condition

Preprints (www.preprints.org) | NOT PEER-REVIEWED | Posted: 18 August 2023 doi:10.20944/preprints202308.1287.v1

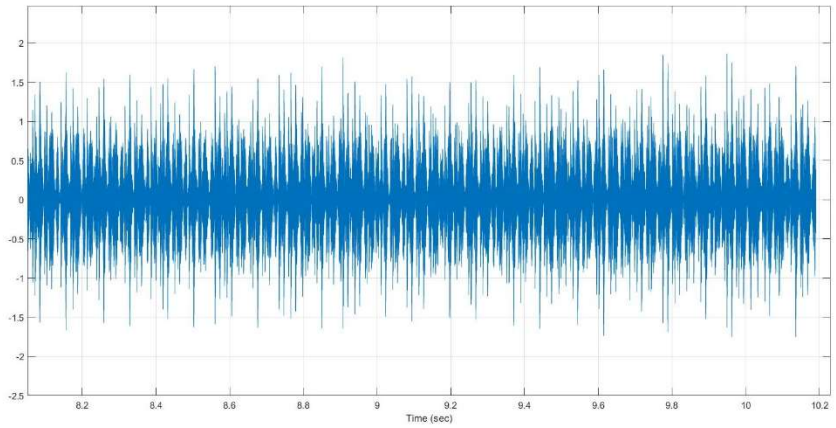

(2b) Inner race defect.

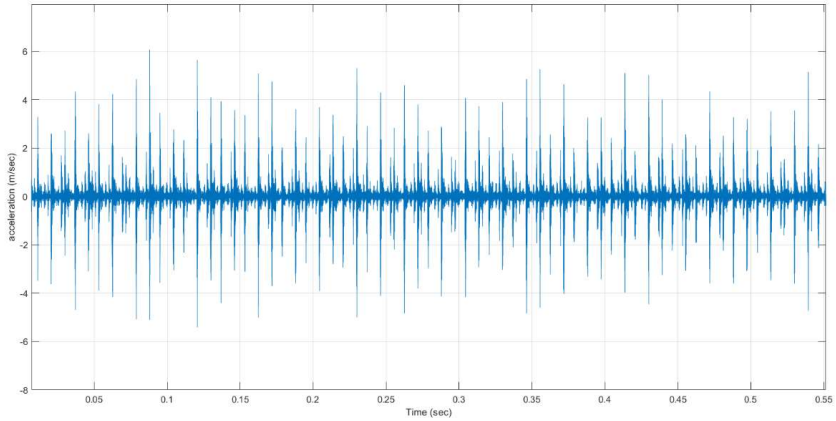

(2c) Outer race defect.

Figure 2. Behaviour of spectrum at different stages of bearing.

3. Methodology

Experimental data were collected from the driver end bearing under two horsepower loads, at a speed of 1800 rpm. The bearing had an inner race fault with a groove width and depth of 38 μm and 12 μm, respectively, as well as an outer race fault with a groove width and depth of 425 μm and 209 μm, respectively. The collected data were analyzed in both the time and frequency domains to extract various features under different operating conditions. Up to fifteen features were extracted from healthy bearings, inner race faulty bearings, and outer race faulty bearings using standard formulae. Finally, ARMA (p, q) modelling techniques were employed to develop a relationship between the extracted features and those of healthy roller bearings. The modelling procedures and simulation steps are discussed in detail below:

Let x_t represent extracted features in various condition for $t = 1,2,3\ldots, n$. Then ARMA (p, q) can be represented as follows

$$x_t = \alpha + \phi_1 x_{t-1} + \cdots + \phi_p x_{t-p} + \varepsilon_t + \theta_1 \varepsilon_{t-1} + \cdots + \theta_q \varepsilon_{t-q} \quad (1)$$

with $\varepsilon_t \sim iid\ (0, \sigma_\varepsilon^2)$ where α represents the features varying intercepts terms. The ϕ_p & θ_q represents the autoregressive and moving average parameters of the features at lag i and j in the equation (1.1) for $i = 1,2,3,\ldots, p$ and $j = 1,2,3,\ldots, q$ which represents varying features for particular lag.

The appropriate model order is determined by analyzing the autocorrelation (ACF) and partial autocorrelation (PACF) functions. The truncation of the ACF reveals the moving average order, while

Preprints (www.preprints.org) | NOT PEER-REVIEWED | Posted: 18 August 2023 doi:10.20944/preprints202308.1287.v1

the truncation of the PACF indicates the autoregressive order of feature representation. Additionally, suitable orders can be identified based on the lowest values of the Akaike (AIC) [29] and Schwarz (SC) [30] information criteria. The AIC is computed using the following equation:

$$AIC(p,q) = \ln\left(\hat{\sigma}^2\,(p,q)\right) + \frac{2(p+q)}{T} \tag{2}$$

Here p, q, $\hat{\sigma}$ and T represent AR component, MA component, the standard deviation of the residuals and the number of the non-missing values in the extracted features respectively.

The Bayesian information criterion for k parameters, L maximum likelihood for n number of extracted features is estimated by

$$BIC(p,q) = 2\ln(L) + k\ln(n) \tag{3}$$

The parameters of the suitable order models were assessed by utilizing the maximum likelihood method. The optimization of the models is acquired on the base of unobservable features.

4. Feature Extraction

Determining which characteristics of machinery are more vulnerable to fault formation and propagation is a challenging task. Additionally, the usefulness of initial features may vary depending on the working environment. This study observed features under varying conditions and loading to designate the degradation of roller bearings in numerous ways. These features indicate the invisible and developing faults of the bearings under study.

To extract the features of healthy and faulty bearings, the recorded vibration data was analyzed using the stochastic resonance technique, which considers the role of random noise in detecting faults. This technique makes it easier to detect faults because noise enhances the signal-to-noise ratio of the bearing's fault signatures. The extracted features are displayed in Figures 3a to 3h for the experimental conditions under study. The skewness displays clear segregation of faulty states from healthy states, and larger skewness is observed in the outer-race fault. The kurtosis for faulty bearings behaves differently at the initial and final stages compared to healthy conditions. Similar behaviour is also observed in the crest and impulse factors. This is because vibration signals for faulty bearings are stronger than the average strength of the signals, and in healthy experimental conditions, the extracted features are consistently compared to faulty conditions. The RMS of the inner race vibration signal has maximum vibration strength, as evident from the graph. On the other hand, the outer and healthy strengthen vibration indices are closely related, indicating the maximum failure of machinery in inner race situations. Marginal features of faulty roller bearings vary up and down from the average or healthy features. Peak-to-peak features in time-domain vibration data display higher variation for faulty bearings compared to healthy bearings because of the changing behaviour in signals due to both faults. The changing shape factors in the vibration signals indicate degradation in both faults with a maximum probability of machinery failure for the inner race.

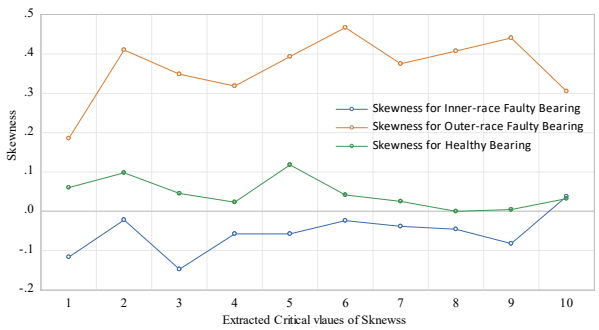

(**a**) Variation in Skewness

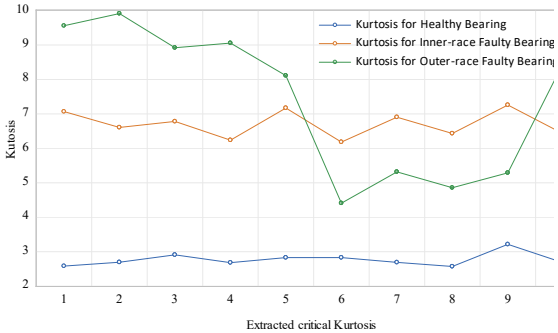

(**b**) Variation in Kurtosis

Preprints (www.preprints.org) | NOT PEER-REVIEWED | Posted: 18 August 2023 doi:10.20944/preprints202308.1287.v1

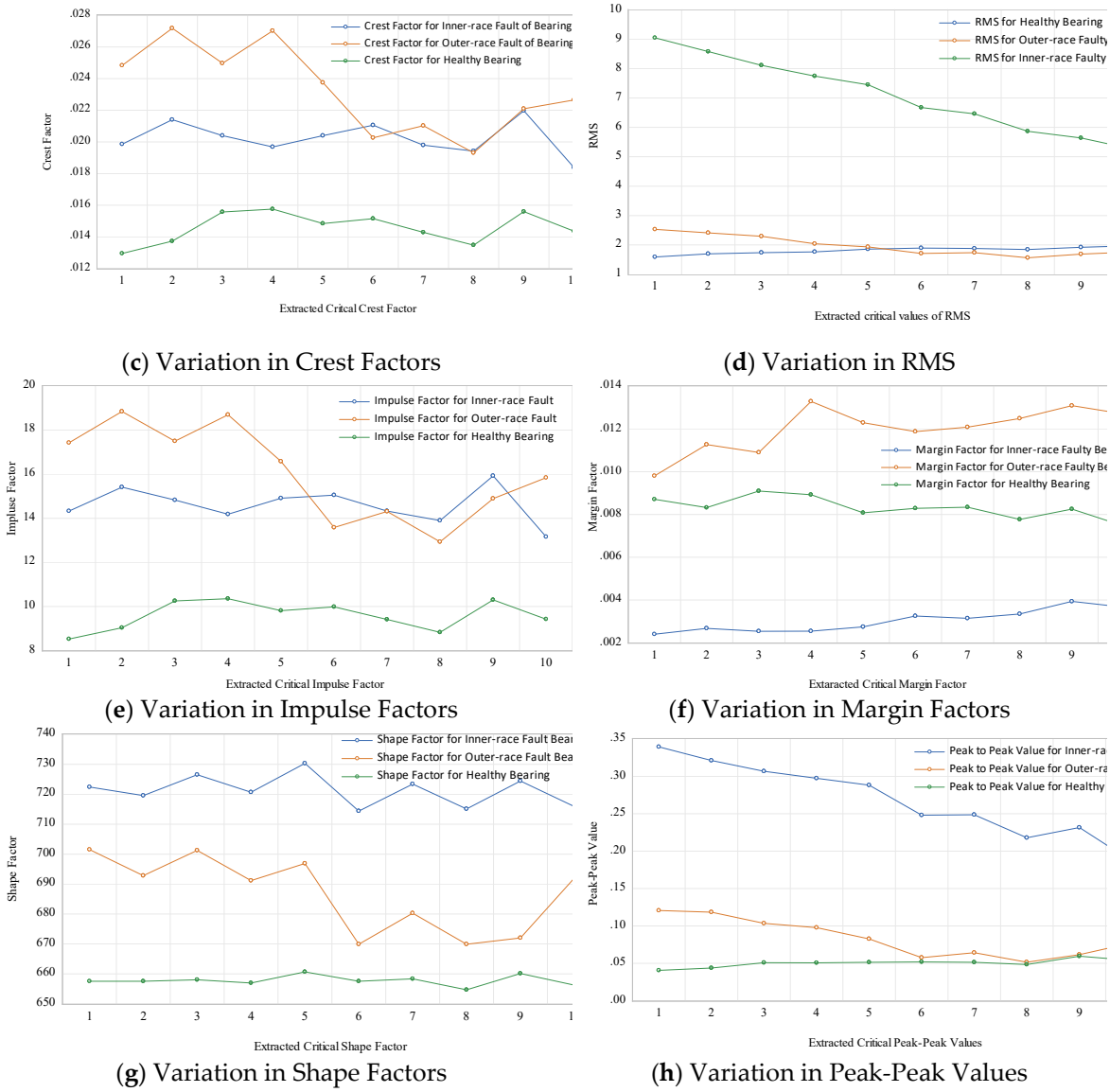

(**c**) Variation in Crest Factors (**d**) Variation in RMS

(**e**) Variation in Impulse Factors (**f**) Variation in Margin Factors

(**g**) Variation in Shape Factors (**h**) Variation in Peak-Peak Values

Figure 3. Variation in extracted feature for understudy experimental conditions.

5. Application of Models to Vibrant Features

In this section extracted features are utilized to construct models by applying stochastic techniques. Firstly models were developed by regressing inner-race faulty features on corresponding healthy features. Secondly, outer-race necessary vibration intensity factors are considered as regressands and analogous healthy factors as regressed. The developed equations with their necessary statistics are represented below:

(i) Stochastic association amongst inner-race falut features with healthy features.

(a) Impulse Factor

$$\tau_t^i = 4.0324 + 1.089\tau_t^h - 0.882\left(\tau_{t-1}^i + \tau_{t-2}^i\right) - 0.99\left(\omega_{t-1}^i + \omega_{t-2}^i + \omega_{t-3}^i\right) + \omega_t^i \quad (4)$$

p-value: (0.042) (0.015) (0.026) (0.047)

$$R^2 = 0.75$$

(b) Crest Factor

$$\lambda_t^i = 0.0056 + 0.986\lambda_t^h - 0.749\left(\lambda_{t-1}^i + \lambda_{t-2}^i\right) - 0.978\left(\omega_{t-1}^{ci} + \omega_{t-2}^{ci}\right) + \omega_t^{ci} \quad (5)$$

p-value: (0.021) (0.0151) (0.0136) (0.057)

Preprints (www.preprints.org) | NOT PEER-REVIEWED | Posted: 18 August 2023 doi:10.20944/preprints202308.1287.v1

$$R^2 = 0.73$$

(c) Shape Factor

$$\theta_t^i = 1.096\theta_t^h - 0.953\theta_{t-1}^i + 0.887\omega_{t-1}^{si} + \omega_t^{si} \quad (6)$$

p-value: (0.001) (0.001) (0.001)

$$R^2 = 0.77$$

(d) Margin Factor

$$\xi_t^i = 0.012 - 1.165\xi_t^h - 0.767\xi_{t-1}^h - 0.884(\omega_{t-1}^{mi} + \omega_{t-2}^{mi}) + \omega_t^{mi} \quad (7)$$

p-value: (0.005) (0.014) (0.056) (0.075)

$$R^2 = 0.75$$

(e) Peak-Peak Factor

$$\rho_t^i = 0.416 - 3.296\rho_t^h + 0.684\rho_{t-1}^h + 0.821(\omega_{t-1}^{pi} + \omega_{t-2}^{pi}) + \omega_t^{pi} \quad ()$$

p-value: (0.006) (0.087) (0.042) (0.099)

$$R^2 = 0.90$$

(f) RMS Value

$$\Phi_t^i = 17.96 - 6.037\Phi_t^h + 0.84\Phi_{t-1}^h + \omega_t^{ri} \quad (9)$$

p-value: (0.012) (0.091) (0.076)

$$R^2 = 0.91$$

(g) Kurtosis

$$\mathrm{K}_{t-1}^i = 2.39\mathrm{K}_t^h - 0.994\mathrm{K}_{t-1}^h - 0.979(\omega_{t-1}^{ki} + \omega_{t-2}^{ki}) + \omega_t^{ki} \quad (10)$$

p-value: (0.001) (0.001) (0.001)

$$R^2 = 0.70$$

(ii) Stochastic association amongst outer-race falut features with healthy features.

(a) Impulse Factor

$$\tau_t^o = 1.731\tau_t^h + 0.635\,\tau_{t-1}^i + 0.99(\omega_{t-1}^i + \omega_{t-2}^i + \omega_{t-3}^i) + \omega_t^i \quad (11)$$

p-value: (0.001) (0.057) (0.056)

$$R^2 = 0.701$$

(b) Crest Factor

$$\lambda_t^0 = 1.639\lambda_t^h + 0.599\lambda_{t-1}^i + 0.87\left(\omega_{t-1}^{ci} + \omega_{t-2}^{ci} + \omega_{t-3}^{ci}\right) + \omega_t^{ci} \quad (12)$$

p-value: (0.001) (0.063) (0.044)

$$R^2 = 0.699$$

(c) Shape Factor

$$\theta_{t-1}^o = 1.0426\theta_t^h + 0.951(\omega_{t-1}^{si} + \omega_{t-2}^{si}) + \omega_t^{si} \quad (13)$$

p-value: (0.001) (0.081)

$$R^2 = 0.68$$

(d) Margin Factor

Preprints (www.preprints.org) | NOT PEER-REVIEWED | Posted: 18 August 2023 doi:10.20944/preprints202308.1287.v1

$$\xi_{t-1}^{o} = 0.024 - 1.51\xi_{t}^{h} - 0.045(\xi_{t-1}^{h} + \xi_{t-2}^{h}) + 0.712\omega_{t-1}^{mi} + \omega_{t}^{mi} \quad (14)$$

p-value: (0.046) (0.049) (0.089) (0.091)

$$R^2 = 0.66$$

(e) Peak-Peak Factor

$$\rho_{t}^{o} = 1.636\rho_{t}^{h} + 0.817(\rho_{t-1}^{h} + \rho_{t-2}^{h}) + 0.873(\omega_{t-1}^{pi} + \omega_{t-2}^{pi} + \omega_{t-3}^{pi}) + \omega_{t}^{pi} \quad (15)$$

p-value: (0.050) (0.069) (0.092)

$$R^2 = 0.68$$

(f) RMS Value

$$\Phi_{t}^{o} = 7.38 - 2.987\Phi_{t}^{h} - 0.524(\Phi_{t-1}^{h} + \Phi_{t-2}^{h}) + \omega_{t}^{ri} \quad (16)$$

p-value: (0.001) (0.002) (0.089)

$$R^2 = 0.84$$

(g) Kurtosis

$$\mathrm{K}_{t}^{i} = 20.17 - 4.586\mathrm{K}_{t}^{h} + 0.718\mathrm{K}_{t-1}^{h} + 0.917(\omega_{t-1}^{ki} + \omega_{t-2}^{ki} + \omega_{t-3}^{ki}) + \omega_{t}^{ki} \quad (17)$$

p-value: (0.071) (0.022) (0.078) (0.088)

$$R^2 = 0.76$$

6. Result & Discussion

The vibration signatures of roller element bearings produce intricate patterns for inner-race and outer-race faults when compared to a healthy state. To establish a relationship between the signals of faulty and healthy bearings, ARMA modelling techniques are employed to determine the optimized parameters.

Initially, equations (1.1) and (1.2) are utilized to determine the appropriate model orders. Table I displays the estimated statistics, including the Akaike Information Criterion (AIC) and Schwarz Criterion (SC), along with their corresponding probability values for suitable ARMA (p, q) orders. The computations are conducted over a range of one to twelve. Subsequently, the stability of the constructed models is ensured through standard statistical techniques, as demonstrated by the necessary statistics provided in the estimated equations' parentheses.

Table 4. Order of Suitable stochastic model with assessed statistics of selection critia.

Models	Order	AIC	BIC
Impulse Factor Inner Race Fault	ARMA(2,3)	2.6516	2.8029
Impulse Factor Outer Race Fault	ARMA(1,3)	4.3337	4.4547
Crest Factor Inner Race Fault	ARMA(2,2)	-10.6074	-10.4561
Crest Factor Outer Race Fault	ARMA(1,3)	-8.8708	-8.7498
Shape Factor Inner Race Fault	ARMA(1,1)	5.6182	5.7392
Shape Factor Outer Race Fault	ARMA(0,2)	7.9342	7.9987

 doi:10.20944/preprints202308.1287.v1

Margin Factor Inner Race Fault	ARMA(1,2)	-12.4488	-12.2974
Margin Factor Outer Race Fault	ARMA(2,1)	-10.4902	-10.3806
Peak-Peak Factor Inner Race Fault	ARMA(2,3)	2.6516	2.4857
Peak-Peak Factor Outer Race Fault	ARMA(1,3)	4.3337	4.4547
RMS Inner Race Fault	ARMA(1,0)	1.7768	1.8978
RMS Outer Race Fault	ARMA(2,0)	-0.4051	-0.2341
Kurtosis Inner Race Fault	ARMA(1,2)	1.1191	1.2067
Kurtosis Outer Race Fault	ARMA(1,3)	4.2627	4.4141

Statistical features of a healthy bearing remain stable over time, whereas inner or outer race faults lead to variations in the extracted features. The magnitude of these statistical features increases with the rate of inner or outer race defect propagation and damage growth, displaying both linear and non-linear tendencies.

The impulse factor for the outer race exhibits a greater difference from a healthy bearing than the inner race, as evidenced by estimated coefficients. This difference arises due to variations in crest factor information for healthy and faulty bearings, extracted from both vibration and acoustic emission signals. The crest factor, which is typically low for a healthy bearing, indicates a smooth and steady vibration signal. In the presence of a fault, the vibration signal becomes more complex, leading to an increase in the crest factor. Consequently, the assessed coefficients of the crest factor vary more in the case of outer race fault than the inner race.

The shape factor of a healthy bearing is generally close to unity, indicating a smooth and steady vibration signal with minimal variation in amplitude. However, the presence of a fault in a bearing leads to changes in the vibration signal's complexity, resulting in a change in the shape factor. The estimated shape factor equation proves useful in improving the accuracy and robustness of fault diagnostics in condition monitoring of rotating machinery.

The margin factor, which represents the difference between the peak and RMS value of the vibration signals, is typically high for a healthy bearing. However, the development of inner or outer race defects leads to changes in these signals, resulting in variations in the margin factor and adjusted coefficients of the estimated models. The peak-to-peak factor is usually low in a healthy bearing, indicating a continuous and smooth vibration signal, whereas it escalates in the case of inner or outer race faults, leading to computed quantities that fluctuate accordingly.

The RMS value, a commonly used statistical measure of the amplitude of a vibration signal, remains relatively stable over time for a healthy bearing and is indicative of the overall level of vibration generated by the bearing. In the presence of a fault, the resulting vibration signal becomes more complex, leading to changes in the RMS value and deviations in the predicted coefficients.

Finally, kurtosis, a statistical measure of the shape of a probability distribution, is often used in vibration analysis and condition monitoring of rotating machinery, including bearings, as an indicator of the presence of impulsive signals commonly associated with bearing faults. The kurtosis value of a healthy bearing is relatively low due to the smooth functioning of the roller bearing. However, fluctuation is observed in the case of inner and outer race faulty bearings due to impulsive vibration signals, which adjust the coefficients accordingly.

Preprints (www.preprints.org) | NOT PEER-REVIEWED | Posted: 18 August 2023 doi:10.20944/preprints202308.1287.v1

7. Conclusion

This study aims to quantify the behaviour of a healthy roller bearing compared to inner and outer race faulty bearings under increasing load using vibration techniques. Vibrant data is collected under various experimental conditions, and signal processing techniques are used to extract significant features. While these features perform smoothly in a healthy bearing, inner or outer faulty roller bearings exhibit a characteristic peak or notch at the fault frequency or its harmonic due to the presence of the fault. Stochastic model equations have been developed by regressing inner and outer race faulty bearing features to healthy bearing features discretely at various experimental conditions. The optimized and suitable model is assessed using stochastic modelling techniques. The computed stochastic coefficients provide important insights into the association of healthy bearing features with inner and outer race faulty bearing structures. These estimated models are helpful in predicting the remaining useful life of roller element bearings with inner and outer race faults, and they can support maintainers in developing effective maintenance strategies to minimize the risk of failure and maximize the machinery's lifespan.

Nomenclatures

λ_t^i =Impulse factor for Inner-race Fault
λ_t^o =Impulse factor for Outer-race Fault
λ_t^h = Impulse factor for Healthy state
ω_t^i = Inner-race impulse factor white-noise term with $\omega_t^i \sim iid(0, \delta^2_{\omega_t^i})$
λ_t^i = Crest factor for Inner-race Fault
λ_t^o = Crest factor for Outer-race Fault
λ_t^h = Crest factor for Healthy state
ω_t^{ci} = Inner-race crest factor white-noise term with $\omega_t^{ci} \sim iid\left(0, \delta^2_{\omega_t^{ci}}\right)$
θ_t^i = Shape factor for Inner-race Fault
θ_t^o = Shape factor for Outer-race Fault
θ_t^h = Shape factor for Healthy state
ω_t^{si} = Inner-race shape factor white-noise term with $\omega_t^{si} \sim iid\left(0, \delta^2_{\omega_t^{si}}\right)$
ξ_t^i = Margin factor for Inner-race Fault
ξ_t^o = Margin factor for Outer-race Fault
ξ_t^h = Margin factor for Healthy state
ω_t^{mi} = Inner-race margin factor white-noise term with $\omega_t^{mi} \sim iid\left(0, \delta^2_{\omega_t^{mi}}\right)$
ρ_t^i = Peak to peak factor for Inner-race Fault
ρ_t^o = Peak to peak factor for Outer-race Fault
ρ_t^h = Peak to peak factor for Healthy state
ω_t^{pi} = Inner-race Peak to peak factor white-noise term with $\omega_t^{pi} \sim iid\left(0, \delta^2_{\omega_t^{pi}}\right)$
Φ_t^i = RMS for Inner-race Fault
Φ_t^o = RMS for Outer-race Fault
Φ_t^h = RMS for Healthy state
ω_t^{ri} = Inner-race RMS white-noise term with $\omega_t^{ri} \sim iid\left(0, \delta^2_{\omega_t^{ri}}\right)$
K_t^i = Kurtosis for Inner-race Fault
K_t^o = Kurtosis for Outer-race Fault
K_t^h = Kurtosis for Healthy state
ω_t^{ki} = Inner-race kurtosis white-noise term with $\omega_t^{ki} \sim iid\left(0, \delta^2_{\omega_t^{ki}}\right)$

References

1. Liu, R., Yang, B., Zio, E., & Chen, X. (2018). Artificial intelligence for fault diagnosis of rotating machinery: A review. Mechanical Systems and Signal Processing, 108, 33-47. https://doi.org/10.1016/j.ymssp.2018.02.016
2. Hoang, D. T., & Kang, H. J. (2019). Rolling element bearing fault diagnosis using convolutional neural network and vibration image. Cognitive Systems Research, 53, 42-50. https://doi.org/10.1016/j.cogsys.2018.03.002
3. Jia, F., Lei, Y., Lin, J., Zhou, X., & Lu, N. (2016). Deep neural networks: A promising tool for fault characteristic mining and intelligent diagnosis of rotating machinery with massive data. Mechanical Systems and Signal Processing, 72-73, 303-315. https://doi.org/10.1016/j.ymssp.2015.10.025

4. Meng, Z., Zhan, X., Li, J., & Pan, Z. (2018). An enhancement denoising autoencoder for rolling bearing fault diagnosis. Measurement, 130, 448-454. https://doi.org/10.1016/j.measurement.2018.08.010
5. Jiang, G., He, H., Yan, J., & Xie, P. (2019). Multiscale convolutional neural networks for fault diagnosis of wind turbine gearbox. IEEE Transactions on Industrial Electronics, 66(4), 3196-3207. https://doi.org/10.1109/TIE.2018.2844805
6. Wang, H., Li, S., Song, L., & Cui, L. (2019). A novel convolutional neural network based fault recognition method via image fusion of multi-vibration-signals. Computers in Industry, 105, 182-190. https://doi.org/10.1016/j.compind.2018.12.013
7. Sun, M., Wang, H., Liu, P., Huang, S., & Fan, P. (2019). A sparse stacked denoising autoencoder with optimized transfer learning applied to the fault diagnosis of rolling bearings. Measurement, 146, 305-314. https://doi.org/10.1016/j.measurement.2019.06.029
8. Meng, Z., Guo, X., Pan, Z., Sun, D., & Liu, S. (2019). Data segmentation and augmentation methods based on raw data using deep neural networks approach for rotating machinery fault diagnosis. IEEE Access, 7, 79510-79522. https://doi.org/10.1109/ACCESS.2019.2923417
9. Hussain, M., Mansoor, A., Qureshi, S., & Nisar, S. (2018). Bearing degradation prognosis using structural break classifier. Mechanika, 24(4), 456-461. https://doi.org/10.5755/j01.mech.4.24.20740
10. Yan, R., & Gao, R. X. (2005). An efficient approach to machine health diagnosis based on harmonic wavelet packet transform. Robotics and Computer-Integrated Manufacturing, 21, 291-301.
11. Conforto, S., & D'alessio, T. (1999). Spectral analysis for non-stationary signals from mechanical measurements: a parametric approach. Mechanical Systems and Signal Processing, 13, 395-411.
12. Wang, G., Luo, Z., Qin, X., Leng, Y., & Wang, T. (2008). Fault identification and classification of rolling element bearing based on time-varying autoregressive spectrum. Mechanical Systems and Signal Processing, 22, 934-947.
13. Zhang, Y., & Ai, S. (2008). EMD based envelope analysis for bearing faults detection. In Intelligent Control and Automation, 2008. WCICA 2008. 7th World Congress on (pp. 4257-4260). IEEE.
14. Miao, Q., Wang, D., & Pecht, M. (2011). Rolling element bearing fault feature extraction using EMD-based independent component analysis. In Prognostics and Health Management (PHM), 2011 IEEE Conference on (pp. 1-6). IEEE.
15. Saidi, L., Ali, J. B., & Fnaiech, F. (2014). Bi-spectrum based-EMD applied to the nonstationary vibration signals for bearing faults diagnosis. ISA transactions, 53, 1650-1660.
16. Zheng, J., Cheng, J., & Yang, Y. (2014). Multiscale Permutation Entropy Based Rolling Bearing Fault Diagnosis. Shock and Vibration, 2014, 1-10.
17. Li, X., & Liang, M. (2019). Bearing fault diagnosis using a hidden Markov model based on vibration signals. IEEE Access, 7, 105151-105160.
18. Dong, J., & Chen, J. (2018). Bearing fault diagnosis based on the hidden Markov model and the support vector machine. Measurement, 128, 354-361.
19. Qiu, Z., Cao, L., & Li, X. (2018). Bearing fault diagnosis using a Markov chain model and improved ensemble empirical mode decomposition. Measurement, 117, 167-176.
20. Li, H., Liang, M., & Li, X. (2017). Bearing fault diagnosis based on a hidden Markov model and multiscale permutation entropy. Mechanical Systems and Signal Processing, 92, 432-447.
21. Guo, W., Chen, J., & Dong, J. (2017). Bearing fault diagnosis based on hidden Markov model with hybrid feature extraction. Measurement, 97, 96-105.
22. Yang, X., & Cao, H. (2016). Fault diagnosis of rolling bearings using a hidden Markov model based on wavelet packet decomposition. Measurement, 85, 63-71.
23. Zhao, Y., & Tang, Y. (2015). Bearing fault diagnosis based on an improved hidden Markov model. Journal of Vibro-engineering, 17(6), 2926-2938.
24. Alshadli, D., & Liu, R. (2021). Bearing Fault Diagnosis Using a Regime-Switching Model-Based Vibration Signal Analysis. IEEE Access, 9, 114369-114378.
25. Ma, X., Zhang, D., & Sun, C. (2019). Bearing fault diagnosis using a regime-switching model based on vibration signals. Mechanical Systems and Signal Processing, 116, 517-528.
26. Sun, C., Chen, S., & Zhang, D. (2018). Bearing fault diagnosis based on a regime switching model and empirical mode decomposition. Measurement, 120, 81-90.
27. Wang, C., He, Z., & Zhang, Y. (2018). Bearing Fault Diagnosis under Variable Speed Conditions Using a Regime Switching Model Based on EMD and ELM. Mathematical Problems in Engineering, 2018, 1-12.
28. Peng, Z., Huang, H., & Liu, Y. (2017). Bearing fault diagnosis based on a variable state dimension hidden semi-Markov model. Measurement Science and Technology, 28(6), 065008.

29. Akaike, H. (1969) 'Fitting autoregressive model models for prediction', Annals of the Institute of Statistical Mathematics, 21, pp. 243-247.
30. Schwarz, G. (1978) 'Estimating the dimension of a model', Annals of Statistics, 6, pp. 461-464.